COBEM 99
XV Congresso Brasileiro de Engenharia Mecânica
15th Brazilian Congress of Mechanical Engineering
22 - 26 de Novembro de 1999 / November 22 - 26, 1999 Águas de Lindóia, São Paulo,

A STUDY OF AXISYMMETRIC JETS WITH APPLICATION TO THE VLS SYSTEM

Daniel Strauss
Centro Técnico Aeroespacial, Instituto Tecnológico de Aeronáutica
CTA/ITA/IEAA – 12228-900 – São José dos Campos, SP, Brasil
João Luiz F. Azevedo
Centro Técnico Aeroespacial, Instituto de Aeronáutica e Espaço
CTA/IAE/ASE-N – 12228-904 – São José dos Campos, SP, Brasil

Abstract. *Axisymmetric, turbulent, viscous flow simulations over the first Brazilian satellite launcher, the VLS, are presented. The emphasis of the work is on multiblock calculations for afterbody flows with propulsive jets. A brief description of the numerical method, based on the Beam and Warming implicit approximate factorization algorithm, as well as of the multiblock implementation is presented. Turbulence closure is obtained in the present case through the use of the Baldwin and Barth one-equation turbulence model. Results for various jet pressure ratios and freestream Mach number flows are discussed. The results obtained demonstrated an excellent qualitative agreement and also a very good quantitative agreement with the available data. Results for flow conditions representative of actual VLS flight are also presented and discussed.*

Keywords: *VLS, Axisymmetric jets, Turbulent flow, Multiblock grids, Finite differences.*

1. INTRODUCTION

The present work is inserted in the context of a larger development program which is aimed at implementing the computational tools that would allow the simulation of realistic launch vehicle flows. In this capacity, the work has to consider turbulent viscous flows, even allowing for extensive regions of separated flow, over fairly complex configurations. Moreover, the existence of rocket engine jet plumes, and their interactions with the external aerodynamic flow, also has to be considered for a complete description of the flight environment. Hence, the implementation and validation of a CFD capability which could handle turbulent flows at afterbody regions is the primary focus of the work here described. This emphasis is on the application of existing turbulence models to particular configurations and flow conditions which are representative of a real engineering problem of interest at the institutions here represented.

A great deal of the CFD development work performed at these institutions is directed towards needs generated by the aerodynamic and aerothermodynamic design of the first Brazilian satellite launcher, the VLS. The starting point for the work here reported was the need to numerically investigate afterbody flows for the VLS system and, in particular, the interaction between the external flow and the plumes from the rocket motor nozzles. Due to the complexity of the geometry in the afterbody region, and with the objective of keeping the codes as modular as possible while still remaining with a structured grid approach, the decision was made to extend

the existing capability (Azevedo, Menezes and Fico, 1995, 1996) in the direction of implementing multiblock techniques. This capability included the possibility of accurately simulating turbulent viscous flows over axisymmetric launch vehicle configurations.

The multiblock extension was described in Azevedo, Strauss and Ferrari (1997) together with some initial results for afterbody flows without a propulsive jet. The work discussed here will extend the validation of these so-called base flow cases, as well as discuss in detail the analysis of afterbody flows including a propulsive jet. The validation effort involves the comparison of numerical results with available experimental data and the study of some numerical effects on the quality of the solutions obtained. Different turbulence models (Azevedo, Menezes and Fico, 1996) were tested within the context of the overall development effort. However, the discussion here will concentrate on the results with the Baldwin and Barth (1990) one-equation model, since the previous experience (Azevedo, Strauss and Ferrari, 1997) with afterbody flows has demonstrated that this model yields superior behavior for the problems at hand.

2. THEORETICAL FORMULATION

The flowfields over the VLS at zero angle of attack are modeled by the azimuthal-invariant, Reynolds-averaged Navier-Stokes equations (Nietubicz, Pulliam and Steger, 1979, Deiwert, 1984, and Zdravistch and Azevedo, 1990). For the case of no body rotation, these equations can be written in general curvilinear coordinates as

$$\frac{\partial \overline{Q}}{\partial \tau} + \frac{\partial \overline{E}}{\partial \xi} + \frac{\partial \overline{F}}{\partial \eta} + \overline{H} = \frac{M_\infty}{Re}\left(\frac{\partial \overline{E}_v}{\partial \xi} + \frac{\partial \overline{F}_v}{\partial \eta} \right) \ . \tag{1}$$

Here, $\overline{Q}$ is the vector of conserved variables, $\overline{E}$ and $\overline{F}$ are the inviscid flux vectors, $\overline{E}_v$ and $\overline{F}_v$ are the viscous flux vectors, and $\overline{H}$ is the axisymmetric source term. The form of these algebraic vectors can be found, for instance, in Zdravistch and Azevedo (1990) and Fernández (1990). In the previous expressions, the usual notation in Fluid Mechanics is being adopted. Moreover, a suitable nondimensionalization of the governing equations is assumed in order to write Eq. (1). In the present case, the choice of reference state proposed in Pulliam and Steger (1980) is adopted. In this equation, M_∞ is the freestream Mach number and the Reynolds number is defined in its usual form as

$$Re = \frac{\ell \rho_\infty q_\infty}{\mu_\infty} \ , \tag{2}$$

where ℓ is the reference length, ρ_∞ is the freestream density, q_∞ is the magnitude of the freestream velocity vector, and μ_∞ is the molecular viscosity coefficient at the freestream temperature. Expressions for the required metric terms and for the Jacobian of the coordinate transformation can be found in Deiwert (1984) and Fernández (1990), among other references.

The correct account for the viscous effects in the present case involves the implementation of an appropriate turbulence closure model. Initial results for base flow cases (Azevedo, Strauss and Ferrari, 1997) have indicated that a turbulence model at least as complex as the Baldwin and Barth (1990) model is necessary for the present applications. Therefore, all results to be reported here have used this model.

The Baldwin and Barth (1990) model is a one-equation model which attempts to avoid the need to compute algebraic length scales, without having to resort to more complex two-equation, or k–ϵ type models. The model was implemented in the present code precisely as described in Baldwin and Barth's original work. The extension of the model for compressible flows was obtained simply by multiplying the kinematic turbulent viscosity coefficient by the local density. Moreover, the turbulence model equation is solved separately from the other governing equations in a loosely coupled fashion. This procedure was adopted in order to avoid having to modify the flux Jacobian matrices and the overall structure of the flow solution algorithm which had been previously implemented. The multiblock capability has not caused any added complexity to the

form of implementing this turbulence model. Moreover, the treatment of the model boundary conditions at block interfaces was performed in similar fashion to the other flow equations.

3. NUMERICAL IMPLEMENTATION

The governing equations were discretized in a finite difference context on a structured quadrilateral mesh which would conform to the body. The computational mesh could be formed by as many patched blocks as necessary to discretize the geometry. The mesh generation within each block could, in principle, be performed in a completely independent fashion. However, for all cases studied in the present work, there was a definite attempt to guarantee some continuity of the mesh spacing across contiguous blocks. Moreover, the block division is such that each side of a block has a single type of boundary condition. The details of the multiblock implementation are described in Azevedo, Strauss and Ferrari (1997).

The Beam and Warming (1978) implicit approximate factorization scheme (see also Pulliam and Steger, 1980) was used, with the implicit Euler method selected for the time march. As usual with the Beam and Warming algorithm, the spatial derivatives were centrally differenced using three-point, second-order finite difference operators. Discretization of the viscous terms uses the so-called midpoint operators in order to obtain a compact finite difference stencil at each point and avoid the need for a different discretization of these terms close to block computational boundaries.

Since a central difference spatial discretization method is being used in the present case, artificial dissipation terms must be added to the formulation in order to control nonlinear instabilities. The present version of the code uses the Turkel and Vatsa (1994) scalar model. This model is scalar and nonlinear, but it is non isotropic since the scaling of the artificial dissipation operator in each coordinate direction is weighted by its own spectral radius of the corresponding flux Jacobian matrix. Implicit artificial dissipation terms were implemented as described in Azevedo, Fico and Ortega (1995). In this approach, only second-difference terms are added in the left-hand side operators, but the coefficients used are obtained by the summation of both the second and fourth-difference term coefficients in order to avoid zero artificial dissipation on smooth regions of the flow.

Variable time stepping was used in order to accelerate convergence to steady state. The implementation of the variable time step option, or constant CFL option, also follows the work in Azevedo, Fico and Ortega (1995). All boundary conditions were treated explicitly in the cases analyzed in this work, including boundaries between computational blocks. The authors believe that this may have caused an effect on the maximum CFL number allowed before the codes would become numerically unstable. Nevertheless, it was considered that it was worth paying the extra costs in terms of computational time instead of further modifying the available codes (Azevedo, Menezes and Fico, 1996) in order to include implicit boundary conditions. In any event, the several computations performed did not show any evidence of stability region limitation that could clearly be attributed to explicit boundary condition treatment. One should further realize that the approximate factorization procedure introduces an error which is of order Δt^2. Hence, there would always be a limitation in the maximum CFL number allowed with the present flow solver algorithm.

4. BOUNDARY CONDITIONS

For the axisymmetric simulations, the types of boundary conditions that should be considered include: solid wall, centerline or symmetry, far field, (downstream) exit plane, jet exit, and block interface boundary conditions. Wall boundary conditions are obtained by imposing no slip at the wall, zero normal pressure gradient and by assuming the wall to be adiabatic. The centerline, both upstream and downstream of the body, is a singularity of the coordinate transformation in the axisymmetric case. Hence, some special treatment of this type of boundary is necessary

because the governing equations can never be solved at the centerline itself. Two different approaches have been implemented in the present case. The first approach considers a line of computational points "on the other side" of the centerline in order to impose symmetry boundary conditions along this line. In this case, there are no computational points along the centerline itself. The other approach treats the centerline as the actual computational boundary and, therefore, there are computational points along the centerline. These points, however, have to receive special treatment in order to avoid divisions by zero and, again, one must remember that the equations can never be solved at the centerline itself. The test performed in the context of the present work indicated that actually having points along the upstream and downstream centerlines, i.e., the second approach previously discussed, yielded a more robust algorithm.

Far field conditions simply assume freestream values can be specified at this computational boundary. This is possible in the present case because the far field boundary is typically located fairly far away from the body. Downstream conditions are based on the concept of one-dimensional characteristic relations (Azevedo, Fico and Ortega, 1995) in order to determine the number of variables which should be extrapolated at this boundary. For a subsonic downstream boundary, the static pressure is fixed and all other quantities at the boundary are obtained by zero-th order extrapolation of their respective values in the adjacent interior point. All flow variables are extrapolated from the adjacent interior point for a supersonic outflow. The jet boundary conditions follow the same reasoning based on characteristic relations. From the point of view of the present computational domain, the jet is seen as a "supersonic" entrance (Azevedo, Fico and Ortega, 1995), since only sonic and supersonic jets were considered in this work. Therefore, all jet properties are specified at this type of boundary.

The treatment of block interfaces is discussed in detail in Azevedo, Strauss and Ferrari (1997) and it will only be briefly outlined here. As discussed in the cited reference, the computational capability here implemented uses patched multiblock grids. The basic ideas underlying this development were that each block should be able to internally identify the types of boundaries on its four sides and that each side should consist of one single type of boundary. The first requirement was introduced in order to make the code implementation modular in the sense that there are no specific tests for any particular block. The second requirement was meant to simplify the implementation of boundary conditions and turbulence models. Moreover, all computational blocks are constructed such that there is an exact two-point overlap between two adjacent blocks. Since the equations are actually solved only at interior grid points, within each block, this two-point overlap ensures that they are solved at all interior points.

5. RESULTS AND DISCUSSION

In a previous effort (Azevedo, Strauss and Ferrari, 1997), the authors have presented the validation of the multiblock extension to an existing axisymmetric, thin-layer Navier-Stokes solver for launch vehicle flows. Azevedo, Strauss and Ferrari (1997) also presented initial studies of afterbody flows for the launch vehicle configurations. However, almost all calculations presented in that reference consider a vehicle without a propulsive jet, i.e., the afterbody flow is essentially the flow over a flat base. These simulations were, nevertheless, instrumental in adjusting turbulence models and grid topologies for turbulent afterbody simulations. A fairly extensive study of base flow cases was included in the same reference in an attempt to validate the simulation capability implemented prior to tackling the more challenging cases in which a propulsive jet is considered.

A typical initial mesh used for the afterbody simulations with the propulsive jet is shown in Fig. 1. The grid shown in Fig. 1 is actually composed of 4 grid blocks. The first two blocks discretize the forebody portion of the vehicle, the third block comprises the region downstream of vehicle base with a "height" equal to the afterbody radius, and the fourth block completes the computational domain. It is important to observe the level of grid refinement in the near wake region. If one compares the grids typically used in Azevedo, Strauss and Ferrari (1997)

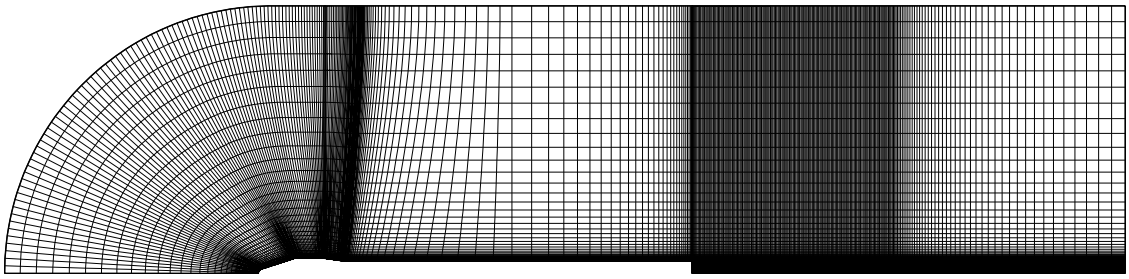

Figure 1: Overall view of a typical initial grid used for the afterbody simulations with jet.

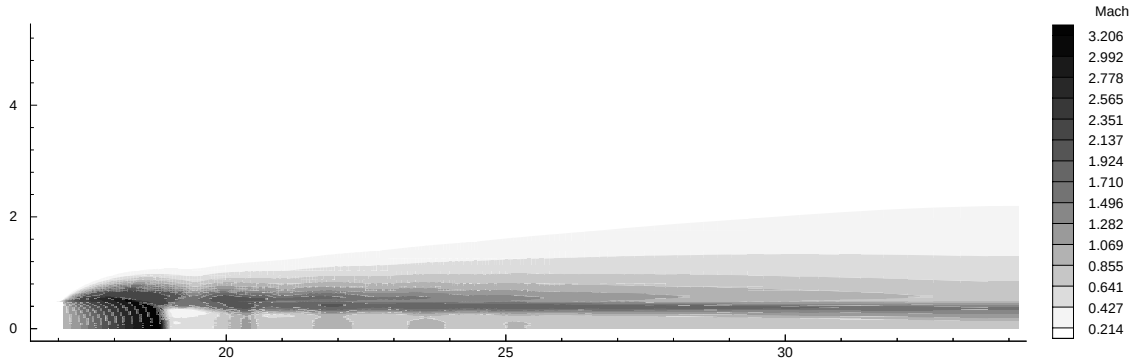

Figure 2: Mach number contours in the wake region for the case $M_{jet} = 1.0$, $M_\infty = 0.01$ and $p_{jet}/p_\infty = 4$.

with, for instance, the one shown in Fig. 1, it becomes evident that the latter has a much less stringent refinement in the near wake region. The reason for this is associated with the fact that the computations in the cited reference were concerned with base flows. Hence, one had to provide adequate refinement in the base-normal direction in order to resolve viscous gradients in that direction. In the present case, the requirement for grid refinement in this direction is lessened because there is no base, but a jet coming out of the base.

A typical result obtained for a free jet, i.e., a jet discharging in a still atmosphere, is presented in Fig. 2. This case considers a sonic jet discharging in a freestream flow with $M_\infty = 0.01$ and with a jet to freestream static pressure ratio of 4. Figure 2 presents Mach number contours in the wake region of the flow. One must observe that, since the authors are using a compressible formulation for the present simulations, it was not possible to consider the external flow with zero velocity. The nondimensionalization adopted yields terms which are divided by the freestream Mach and, hence, if M_∞ is identical to zero, there are numerical problems. Therefore, the procedure adopted here was to consider a very small freestream Mach number, for instance, $M_\infty = 0.01$, in order to simulated the free jet cases. Clearly, the major interest for launch vehicle flows is in cases with a non-zero freestream flow. However, the vast majority of the data available in the literature for validation of such calculations considers free jets. Hence, results for some free jet cases are discussed in the present study in order to validate the capability implemented against data available in the literature.

A more quantitative comparison of the results shown in Fig. 2 will be presented in the forthcoming paragraphs. For this comparison, a sketch of the expected jet structure in the vicinity of the jet exit is indicated in Fig. 3. In this figure, d is the diameter of the jet which, in the present case, is assumed to be equal to the diameter of the afterbody, δ is the angle of the initial slope of the jet expansion region, s is the diameter of the normal shock, ℓ is the longitudinal distance of the normal shock from the jet exit, and w is the total length of the first supersonic flow region. It must be noticed that the jet structure shown in Fig. 3 is mostly

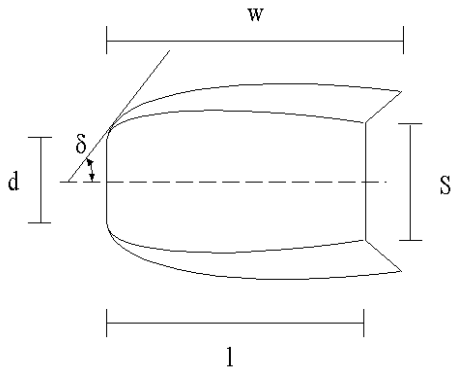

Figure 3: Sketch of the expected jet structure in the vicinity of the jet exit for a free jet.

concerned with free jets. For the cases with a high speed freestream flow, the jet expansion is somewhat inhibited by the freestream flow and the jet structure can be different. At this point, it should be also emphasized that the flow features present in the solution of Fig. 2 are in very good agreement with the expected behavior for this case. The first barrel shock at approximately two body diameters downstream of the jet exit can be clearly seen in Fig. 2.

Although various simulations for free jet cases with jet to freestream pressure ratios up to 4 were performed and good results, similar to those shown in Fig. 2, could be obtained with grids similar to the one shown in Fig. 1, problems arose when the pressure ratio was increased. For such higher pressure ratio cases, the crossflow extension of the normal shock ending the first supersonic region downstream of the jet also increases. Hence, this normal shock starts to cross the region of intense grid refinement in the crossflow direction due to the continuation of the body boundary layer grid. The solutions obtained for these higher pressure ratios started to develop very strange features. The problem was solved with the implementation of a different computational grid topology in the downstream portions of the mesh. Hence, the original mesh in the wake region, shown in Fig. 1, was modified in order to yield an uniform point distribution in the crossflow direction at the downstream boundary. This modified mesh is shown in Fig. 4. This new grid topology was chosen because it causes an increase in the mesh spacing for the points in the region were the problems were observed, and because it can be easily implemented. Clearly, there was some expectation that the previously described problems could have been caused by the rapid variation in the grid size in the crossflow direction as one crosses the portion of the grid which is essentially the continuation of the body boundary layer grid.

Results with the new mesh for the case $M_{jet} = 1.0$, $M_\infty = 0.01$ and $p_{jet}/p_\infty = 10$ are presented in Fig. 5 in terms of Mach number contours. For comparison purposes, the lines dividing the various downstream grid blocks are shown in Fig. 5. The results in this figure are yielding very smooth and well-behaved contours. Problems in the barrel shock, which were present in the original mesh, were fully eliminated by the new grid topology. Hence, the problems observed were caused by having the enlarged normal shock, for the higher pressure ratios, crossing a region of rapidly varying grid spacing and extremely fine grids in the crossflow direction. This, in turn, has caused the addition of excessive amounts of artificial dissipation which destroyed the correct capture of the shock. This conclusion is corroborated by the fact that, with the modified grid, one has to increase the amount of background dissipation available in the code in order to avoid the growth of numerical instabilities.

A comparison of the expected jet structure presented in Fig. 3 with the computational results shown, for instance, in Figs. 2 and 5 indicates that there is good agreement at least qualitatively. A more quantitative comparison of these results is presented in Table 1. The results in Table 1 consider flow conditions with $M_{jet} = 1.0$, $M_\infty = 0.01$ and $T_{jet} = T_\infty$, and three different jet to

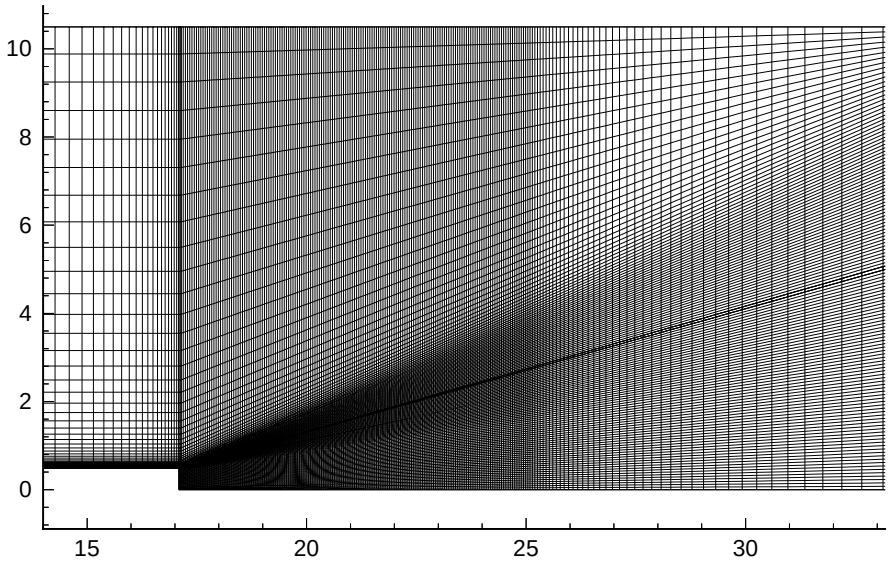

Figure 4: Modified grid used for the afterbody simulations with jet. Figure shows only the detail of the afterbody and wake regions.

Table 1: Comparison of the jet structure near the jet exit for the case $M_{jet} = 1.0$, $M_\infty = 0.01$ and $T_{jet} = T_\infty$.

Parameter	$p_{jet}/p_\infty = 4$		$p_{jet}/p_\infty = 10$		$p_{jet}/p_\infty = 16$	
	Numerical	Experiment	Numerical	Experiment	Numerical	Experiment
w/d	2.3	2.4	3.7	3.6	4.9	4.6
ℓ/d	1.8	1.8	3.1	2.9	3.9	3.7
s/d	0.74	0.64	1.64	1.40	2.20	1.96
δ (deg)	24.4	25.9	44.6	40.2	57.0	48.0

freestream pressure ratios. These results are also indicating a very good quantitative agreement, at least for these three cases. Discrepancies between the present computational results and the experimental data (Love *et al.*, 1959) are usually less than 10%, except for the diameter of the normal shock wave in the two lower pressure ratio cases and the initial slope of the jet expansion region in the highest pressure ratio case. In these cases, the differences are of the order of 15%.

The presence of a freestream flow can significantly affect the structure of the jet. For instance, for the case of a sonic jet with $p_{jet}/p_\infty = 10$ and an outside flow with $M_\infty = 2.0$, one can clearly see in Fig. 6 that the diameter of the normal shock is much smaller than the one obtained in the corresponding case with no external flow, shown in Fig. 5. Moreover, the shock is located further downstream than in the case with no external flow, indicating that the longitudinal extent of the high speed flow is larger for the case shown in Fig. 6. One can also observe in this figure that, since now there is a supersonic freestream, an oblique shock wave is formed at the corner of the body at the jet exit. Although the authors have no experimental data to confirm this result, it is exactly the type of behavior that one should expect to see in such a case.

The computational capability developed was also applied to the simulation of flow conditions which are representative of the actual flight environment for the VLS system. This was an attempt to use the code in more severe conditions that would eventually result in more complex flowfields, thus allowing for an extended knowledge of the code's capabilities. Freestream and jet properties which were representative of the first and second stage flight conditions were used, although the geometric configuration considered here was that of the VLS second stage.

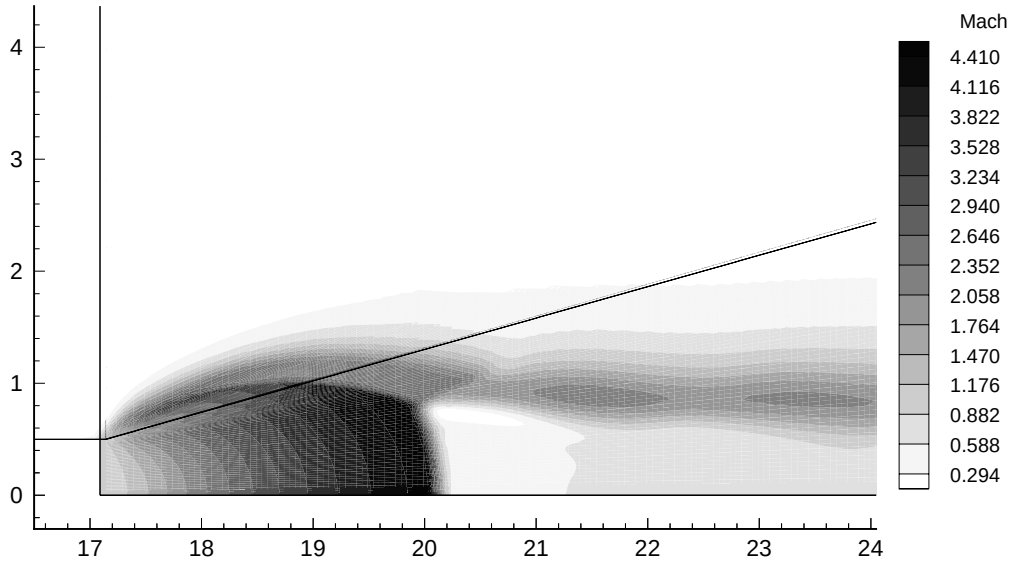

Figure 5: Mach number contours with the new mesh in the near wake region for the case $M_{jet} = 1.0$, $M_\infty = 0.01$ and $p_{jet}/p_\infty = 10$.

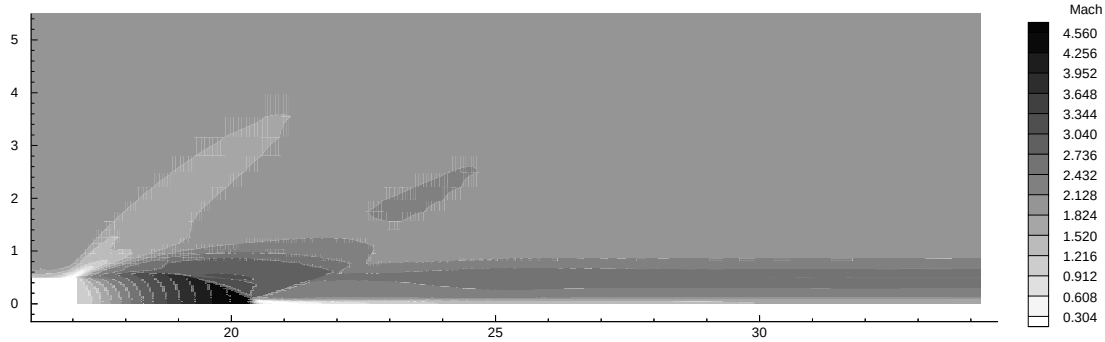

Figure 6: Mach number contours downstream of the jet exit for the case $M_{jet} = 1.0$, $M_\infty = 2.0$ and $p_{jet}/p_\infty = 10$.

The flow conditions which are being associated here to the VLS first stage flight consider $M_\infty = 2.0$, $Re = 20 \times 10^6$, $M_{jet} = 3.3$, $T_{jet}/T_\infty = 7.8$ and $p_{jet}/p_\infty = 1.3$. Mach number contours for this case are presented in Fig. 7. Since the jet to freestream static pressure ratio is close to unity in this case, the jet expansion is small and, therefore, so is the jet plume radial extension. However, since the jet Mach number at the jet exit plane is different from the freestream Mach number, a shear layer is formed which slows down the jet and reduces the thickness of the high Mach number jet core. No shock wave structure is observed in the afterbody region for this case, probably as a consequence of the low jet pressures which, in turn, result in a small expansion and relatively small Mach numbers within the jet.

Flow conditions representative of the VLS second stage flight were much more severe than the ones in the previous case. Freestream and jet properties considered in this case were $M_\infty = 4.9$, $Re = 20 \times 10^6$, $M_{jet} = 4.0$, $T_{jet}/T_\infty = 4.6$ and $p_{jet}/p_\infty = 112$. The Mach number contours for this case are shown in Fig. 8, and the authors point out that the block division lines are also shown in both Figs. 7 and 8 to facilitate the identification of the grid division. One can observe that the jet expansion is very large in this case, and the plume structure seems to be similar to what can be observed, for instance, in Fig. 5. However, the computational domain does not extend far enough downstream in order to capture the normal shock and all the downstream

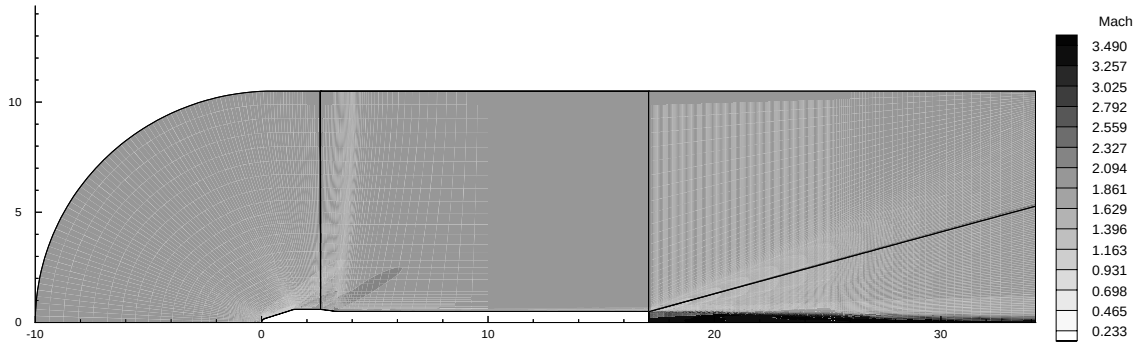

Figure 7: Mach number contours for flow simulation over the VLS using representative first stage flight freestream and jet conditions ($M_\infty = 2.0$, $Re = 20$ million, $M_{jet} = 3.3$, $T_{jet}/T_\infty = 7.8$ and $p_{jet}/p_\infty = 1.3$). Geometric configuration is that of second stage flight.

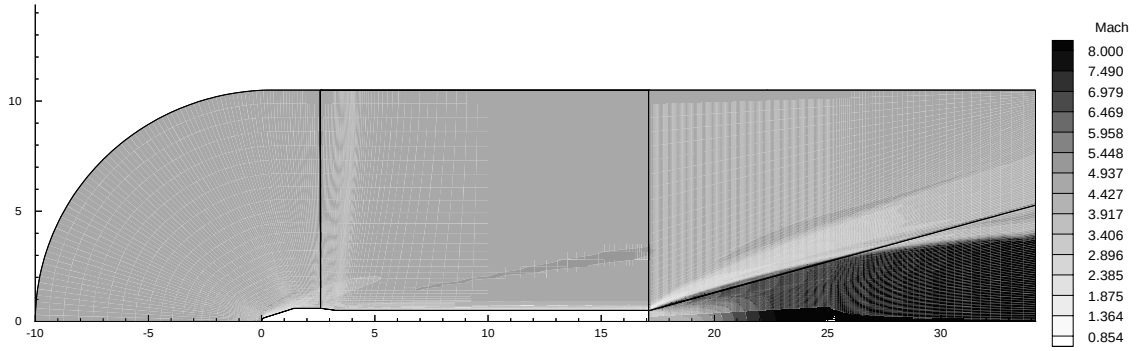

Figure 8: Mach number contours for flow conditions representative of the VLS second stage flight ($M_\infty = 4.9$, $Re = 20$ million, $M_{jet} = 4.0$, $T_{jet}/T_\infty = 4.6$ and $p_{jet}/p_\infty = 112$).

portions of the plume structure. Nevertheless, from the point of view of the accuracy of the solutions here presented, this fact should not cause any problems since the flowfield is completely supersonic throughout the entire exit plane. Therefore, whatever flow structures are supposed to appear downstream of the computational exit plane cannot influence the solution in the present computational domain. Furthermore, as one could expect, the very high jet to freestream static pressure ratio results in a strong expansion downstream of the jet exit, with local Mach numbers within the jet core reaching values as high as 12. The full range of Mach numbers within the jet is not represented in the labels of Fig. 8 in order to allow the reader to see some other features of the flow. Moreover, the rapid jet expansion at its exit station causes the formation of an oblique shock wave in the external flow right at the afterbody edge, as also shown in Fig. 8.

6. CONCLUDING REMARKS

The work presented an effort to implement and validate a CFD simulation capability which could handle turbulent flows at launch vehicle afterbody regions. For such cases, the ability to compute the rocket engine jet plumes and their interactions with the external aerodynamic flow is of fundamental importance in order to simulate the complete flight environment. The present work had as its major objective to introduce propulsive jets in the simulation, since a previous effort had already developed the capability of analyzing afterbody flows without a propulsive jet. The validation effort involved the comparison of numerical results with available experimental data and the study of some numerical effects on the quality of the solutions obtained.

Since the majority of the data in the literature is concerned with free jets, a large number of simulations was initially performed considering jets discharging in a still atmosphere. Due to specific details of code implementation, this was simulated here considering an external freestream with $M_\infty = 0.01$. An extremely good qualitatively agreement was obtained provided that the appropriate mesh topology and adequate levels of artificial dissipation were selected. The quantitative comparison of results for the free jet cases also indicated good agreement with the available data. Discrepancies between the computational results and the experimental data were usually less than 10%. Results with a non-zero freestream Mach number also indicated very good qualitative agreement with the type of behavior that should be expected in this case.

Acknowledgments

The present work was partially supported by Conselho Nacional de Desenvolvimento Científico e Tecnológico, CNPq, under the Integrated Project Research Grant No. 522413/96-0.

REFERENCES

Azevedo, J.L.F., Fico, N.G.C.R., Jr., and Ortega, M.A., 1995, Two-dimensional and axisymmetric nozzle flow computations using the Euler equations, RBCM – J. of the Braz. Soc. Mechanical Sciences, Vol. 17, No. 2, pp. 147-170.

Azevedo, J.L.F., Menezes, J.C.L., and Fico, N.G.C.R., Jr., 1995, An assessment of boundary layer properties for transonic and supersonic flows over the VLS, AIAA Paper 95-1769-CP, Proceedings of the 13th AIAA Applied Aerodynamics Conference, June 19-22, San Diego, CA, Part 1, pp. 41-51.

Azevedo, J.L.F., Menezes, J.C.L., and Fico, N.G.C.R., Jr., 1996, Accurate turbulent calculations of transonic launch vehicle flows, AIAA Paper No. 96-2484-CP, Proceedings of the 14th AIAA Applied Aerodynamics Conference, June 17-20, New Orleans, LA, Part 2, pp. 841-851.

Azevedo, J.L.F., Strauss, D., and Ferrari, M.A.S., 1997, Viscous multiblock simulations of axisymmetric launch vehicle flows, AIAA Paper No. 97-2300, Proceedings of the 15th AIAA Applied Aerodynamics Conference, Atlanta, GA, June 23-26, Part 2, pp. 664-674.

Baldwin, B.S., and Barth, T.J., 1990, A one-equation turbulence transport model for high Reynolds number wall-bounded flows, NASA TM-102847.

Beam, R.M., and Warming, R.F., 1978, An implicit factored scheme for the compressible Navier-Stokes equations, AIAA Journal, Vol. 16, No. 4, pp. 393-402.

Deiwert, G.S., 1984, Supersonic axisymmetric flow over boattails containing a centered propulsive jet, AIAA Journal, Vol. 22, No. 10, pp. 1358-1365.

Fernández, F.Z., 1990, Simulation of aerodynamic flows over cluster type configurations, Master Dissertation, Instituto Tecnológico de Aeronáutica, São José dos Campos, SP, Brazil.

Fletcher, C.A.J., 1988, Computational Techniques for Fluid Dynamics 2. Specific Techniques for Different Flow Categories, Springer-Verlag, Berlin.

Love, E.S., et al., 1959, Experimental and theoretical studies of axisymmetric free jets, NASA Technical Report R-6.

Nietubicz, C.J., Pulliam, T.H., and Steger, J.L., 1979, Numerical solution of the azimuthal-invariant thin-layer Navier-Stokes equations, AIAA Paper 79-0010, 17th Aerospace Sciences Meeting, January 11-14, New Orleans, LA.

Pulliam, T.H., and Steger, J.L., 1980, Implicit finite-difference simulations of three-dimensional compressible flow, AIAA Journal, Vol. 18, No. 2, pp. 159-167.

Turkel, E., and Vatsa, V.N., 1994, Effect of artificial viscosity on three-dimensional flow solutions, AIAA Journal, Vol. 32, No. 1, pp. 39-45.

Zdravistch, F., and Azevedo, J.L.F., 1990, Numerical simulation of high speed flows over complex satellite launchers, Proceedings of the 3rd Brazilian Thermal Sciences Meeting, December 10-12, Itapema, SC, Vol. I, pp. 233-238.